

Thermal shock resistance of yttrium aluminium oxide $Y_3Al_5O_{12}$ thermal barrier coating for titanium alloy

M. A. Almomani^{1*}, M. I. Al-Widyan² and S. M. Mohaidat²

¹ Industrial Engineering Department, Faculty of Engineering, Jordan University of Science and Technology, P.O. Box 3030, Irbid, 22110, Jordan.

² Mechanical Engineering Department, Faculty of Engineering, Jordan University of Science and Technology, P.O. Box 3030, Irbid, 22110, Jordan.

ABSTRACT – The high strength-to-weight ratio of titanium alloys allows their use in jet engines. However, their use is restricted by susceptibility to oxidation at high temperatures. In this study, the possibility of increasing the operating temperature of titanium alloys through using Yttrium Aluminum Oxide (YAG) as a thermal barrier coating material for Ti-6Al-4V substrate is studied. The study concludes that YAG can be utilized to increase the operating temperature of Ti-6Al-4V titanium alloy from around 350 °C to 800 °C due to its low thermal conductivity and phase stability up to its melting point. In addition, its lower oxygen diffusivity in comparison with the standard YSZ material will provide a better protection of the titanium substrate from oxidation. In this work, coating was created using atmospheric plasma spray. X-ray Diffraction (XRD) and Scanning Electron Microscope (SEM) were used to examine coatings' composition and structure. The coating was characterized by thermal shock test, Vickers hardness test and adhesion strength test. X-ray diffraction indicated that the coating was of a partially crystalline $Y_3Al_5O_{12}$ composition. The coating was porous with excellent thermal shock resistance at 800 °C, with a Vickers micro-hardness of 331.35 HV and adhesion strength of 17.6 MPa.

ARTICLE HISTORY

Revised: 26th Sept 2019

Accepted: 16th Oct 2019

KEYWORDS

*Thermal barrier coating;
Yttrium aluminum oxide;
thermal shock resistance*

INTRODUCTION

High operating temperatures of heat engines increase their efficiency. The use of light engines results in lower fuel consumption and less gas emission [1]. Titanium alloys and titanium aluminide are used as high temperature structural materials in aerospace and automotive applications due to their high strength-to-weight ratio, their low density and high corrosion resistance [2-6]. However, the susceptibility of titanium alloys to oxidation at high temperatures results eventually in degradation of the alloys mechanical performance and limit their operating temperature to around 600 °C. Therefore, several methods have been used to increase the operating temperatures of titanium alloys and protect them from oxidation, these methods are based either on bulk modification using alloying elements or using surface modification methods as coating. The former method may negatively affect the mechanical properties of the alloys, whereas the later method can also be used without affecting the mechanical properties of Ti alloys, such coatings include glass coatings and thermal barrier coatings (TBCs) [7,8]. TBCs are utilized in high temperature parts of gas turbines in order to provide thermal protection of the substrates allowing the possibility of increasing their operating temperature and increasing their efficiency [9, 10]. In addition, TBCs can be used to protect the substrate against hot corrosion [11] and attacks by Calcium Magnesium Alumino Silicate (CMAS) attacks [12]. TBCs are usually multi layered structure, in which the top layer is made of ceramic material with low thermal conductivity. Then, a metallic bond coat layer of a nickel based superalloy is used underneath the top coat to enhance adhesion between substrate and top coat and protects the substrate from corrosion and oxidation [13], and a thermally grown oxide layer between the top and the bond coats that forms due to the oxidation of the bond coat [14]. Two main methods are usually used for manufacturing TBCs top coat, namely: Atmospheric Plasma Spray (APS), and Electron Beam Physical Vapor Deposition (EB-PVD) [15]. Other new methods include suspension plasma spray [16] solution precursor plasma spray [17], plasma spray-physical vapor deposition [18] and electrophoretic deposition [19]. Recently, advanced TBCs such as nanostructured TBCs [20] and functionally graded TBCs [21] with enhanced performance were produced. TBC performance can also be enhanced by laser glazing [22]. Yttria Stabilized Zirconia (YSZ) is the most common TBC top coat material that is composed of 6% to 8% of Y_2O_3 added to ZrO_2 . The YSZ has the advantages of low thermal conductivity of 2.1-2.2 W/m.K and high coefficient of thermal expansion of $10.5-11.5 \times 10^{-6} / K$ as well as good chemical and structural stability. However, its application is limited to 1200 °C because the phase transformation that happens at higher temperatures [23]. The use of Yttrium Aluminum Oxide ($Y_3Al_5O_{12}$) known as YAG as a possible TBC material has attracted the interest of researchers, particularly it has outstanding mechanical properties at high temperatures. Both theoretical and experimental studies on YAG were conducted. Experimentally, the thermal conductivity of YAG was found to be 3.2 W/m.K at 1000 °C [24]. Even though, this value is relatively higher than thermal conductivity of the standard YSZ, but YAG had much lower oxygen diffusivity and superior mechanical properties at higher temperatures as compared with standard YSZ and YAG does not undergo

phase change up to its melting temperature [24]. YAG has also superior creep and corrosion resistance [25,26]. YAG performance as a TBC material can be enhanced by doping with Yb^{3+} ions which leads to reduced thermal conductivity and increased coefficient of thermal expansion [27,28]. Therefore, several technologies were used to apply YAG coating such as combustion spray pyrolysis [29], electrostatic spray assisted vapor deposition [33], atmospheric plasma spraying [31,32] and solution precursor plasma spray [33]. Based on our extensive literature search, the synthesis and study of YAG-based TBC for titanium alloys was not conducted before. Hence, this work aims to create a YAG TBC over Ti-6Al-4V alloy using the atmospheric plasma spray process. Ni5Al alloy was used as a bond coat. The performance of the coating at high temperature was analyzed by the thermal shock resistance test while the coating's composition and morphology were characterized using X-ray Diffraction (XRD) and Scanning Electron Microscope (SEM), respectively. Finally, the Vickers hardness, and adhesion strength tests were conducted to test the coating properties.

METHODS AND MATERIALS

Preparation of Coating

In this work, titanium alloy Ti-6Al-4V was selected as a substrate, Ni-5Al that is commercially known as Metco 450 NS with a size of $-90+45 \mu\text{m}$ as the bond coat, and yttrium aluminum oxide (YAG) $Y_3Al_5O_{12}$ as the top coat. Ti-6Al-4V sheet was brought from Titan Engineering, Singapore; the chemical composition of which is provided in Table 1.

Table 1. Chemical composition of Ti-6Al-4V substrate as provided from Titan Engineering supplier.

Element	C	N	Fe	Al	V	O	Ti
Wt. %	0.12	0.008	0.21	6.16	3.96	0.15	Balanced

YAG powder was obtained from LTS Research Laboratories Ltd, Orangeburg NY, USA with the size of -100 mesh and irregular shapes. As provided from the supplier, the chemical composition of the YAG powder with elements having concentration higher than 5 ppm is given in Table 2.

Table 2. Chemical composition of YAG powder showing elements having concentration >5 ppm as provided from LTS research laboratories.

Element	Al	Ca	O	Er	Fe	Y	Ho	Si
ppm	Matrix	7	Matrix	14.1	6.4	Matrix	9	11.7

The substrates were flat 34×28 mm rectangular pieces of 2.54 mm thickness. To prepare the samples for coating, the sample surfaces were roughened by blasting with 20 mesh grit size Al_2O_3 particles, and then cleaned by compressed air. Furthermore, a multi-sample holding fixture was fabricated so that 14 samples can be spray-coated simultaneously. The holding fixture is made of aluminum and designed to rotate about a fixed axis on the machine bed. The samples were mounted on the fixture by using screws adjustable locating plates with the area of interest facing plasma gun.

The coating was prepared at the premises of Jordan Airmotive Company (JALCO) utilizing their atmospheric plasma spray machine equipped with an F4MB plasma spray torch (OerlikonMetco). The bond coat Ni-5Al was sprayed using the standard parameters utilized by JALCO besides those provided by the coating manufacturer OerlikonMetco, Switzerland. As for the top coat, the parameters implemented were obtained from literature [34]. The spray parameters for both bond coat and YAG are listed in Table 3.

Table 3. Atmospheric plasma spray parameters for the Ni-5Al bond coat and YAG top coat.

Parameter	Ni-5Al	$Y_3Al_5O_{12}$
Primary gas flow rate (slpm)	50	45
Secondary gas flow rate (slpm)	10	7
Current (A)	600	650
Carrier gas flow rate (slpm)	2.2	5
Spray distance (mm)	145	120

Initially, the bond coat Ni-5Al with a thickness of around $100 \mu\text{m}$ was sprayed over the substrate. Then, the top coat YAG was sprayed over the bond coat with a thickness of approximately $250 \mu\text{m}$.

Characterization of the Coating

The XRD was conducted using RigakuUltima IV 185 mm X-ray diffractometer using Cu K- α with 0.15418 nm . The scanning range was in the range of 5° to 90° . The XRD was carried out after the sample was heat treated at 950°C for one hour in the as-sprayed condition. The coating microstructure was characterized using Quanta FEG 450 SEM equipped

with X-ray Energy Dispersive Spectroscopy (EDX). To prepare the samples for cross-sectional characterization, they were cut using Metkon Metacut abrasive cutter, and then coated with 8 nm layer of gold using Quorum Q 150R ES.

The thermal shock test was conducted by heating the samples to 800 °C and maintaining that for a 5-minute dwell time followed by quenching them in deionized water at room temperature. The test was repeated for 150 cycles using three samples. Thereafter, the cross-section of the thermally shocked samples was examined using SEM/EDX. The Vickers hardness tester from Shanghai Jiming HVE-5A1 was used to measure the material hardness using 1 kg load and a dwell time of 10 seconds. The adhesion strength test was conducted according to ASTM C633 using a pull of adhesion tester by DFD instruments. The samples were cut to proper dimensions and glued to holding cylinders of the device using F.M 1000 adhesive film. The samples were then placed in the furnace for two hours at 200 °C.

RESULTS AND DISCUSSION

X-ray Diffraction

The XRD patterns for both the as sprayed top coat and the annealed one are shown in Figure 1.

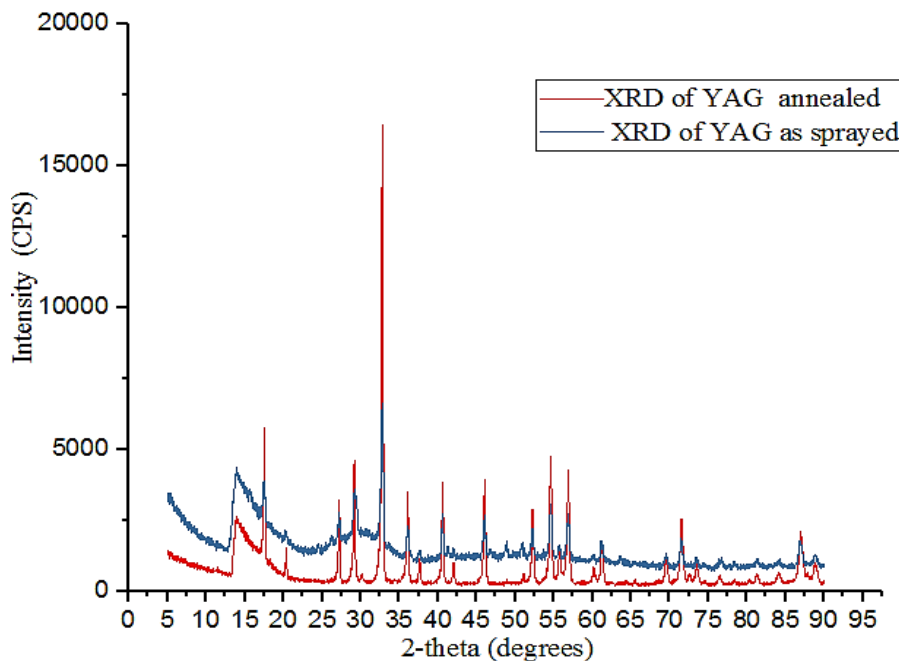


Figure 1. XRD pattern of YAG in the as-sprayed condition and after annealing.

The patterns have peaks at $2\theta^\circ = 18.06, 20.3, 27.22, 29.22, 32.36.08, 41.26, 46.06, 52.24, 54.6, 56.9, 61.26, 71.52, 87.06$. The diffraction patterns of both the as-sprayed and annealed samples confirmed that the top coat is composed of YAG only as determined by Rigaku PDXL XRD analysis software based on International Center for Diffraction Data (ICDD) database [35], and no decomposition or formation of new materials was observed. Figure 1 also shows that the intensities of diffraction peaks for the annealed sample were higher than those of the corresponding peaks in the as-sprayed sample. The rapid cooling of the molten YAG droplet during the solidification caused the as-sprayed coating to be partially amorphous. On the other hand, crystallinity was promoted by the presence of unmelted YAG powder and/or the crystallization of YAG splats during the coatings deposition and solidification [31]. The observed non-crystallinity in $Y_3Al_5O_{12}$ TBCs is expected to reduce its thermal conductivity due to the random nature of thermal transport in disordered amorphous structures that entails strong phonon scattering, according to minimum thermal conductivity model used to predict the thermal conductivity of amorphous solids [32,36]. Hence, the thermal conductivity of the developed YAG TBC is expected to be less than the experimental reported value of the dense crystalline YAG at 800 °C [24] which is about 3.5 W/m.K or the theoretical value predicted by the minimum thermal conductivity model which is 1.59 W/m.K [37].

Morphology of the Coating Cross-Section

Figure 2 provides a SEM image of the sample's cross-section showing topcoat, bond coat and the substrate. It indicates that the bond coat-substrate and top coat-bond coat interfaces were complex causing better mechanical interlocking and strong bonding. Figure 2 suggests that interfacial cracks were non-existent. Further pores were distributed through the top coat with few pores at the substrate bond coat interface, examples of these pores are labeled and enclosed in rectangles in Figure 2.

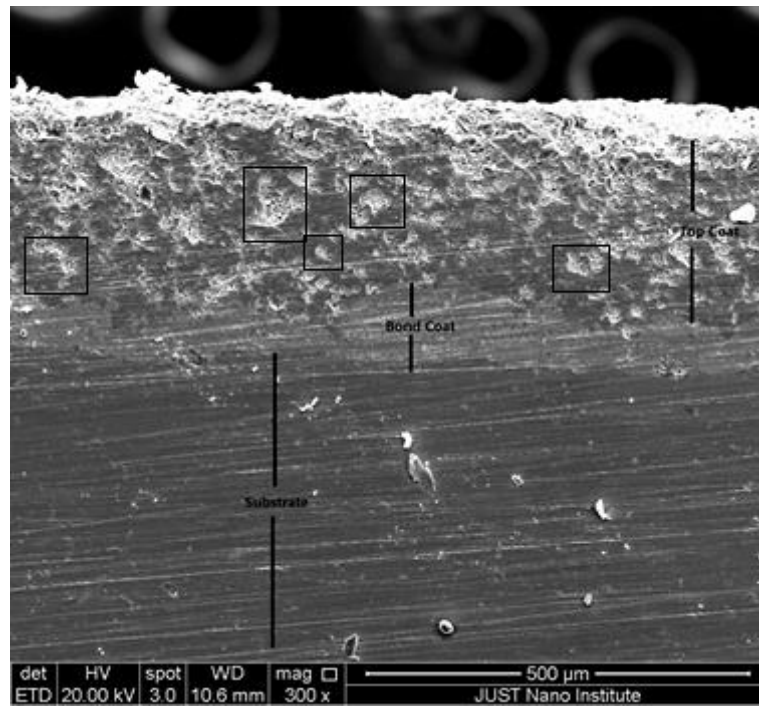


Figure 2. SEM image of the sample's cross-section showing topcoat, bond coat and the substrate.

These pores will act to reduce the thermal conductivity of TBC [38], and increase its strain tolerance leading to increased spallation resistance [39] and thermal shock resistance [40]. Figure 3(a) indicates that the pores contain unmelted or partially melted particles with different shapes and sizes and that the coarse pores are connected with micro channels. Unmelted and partially melted particles are more visible at higher magnifications as can be seen in Figure 3(b).

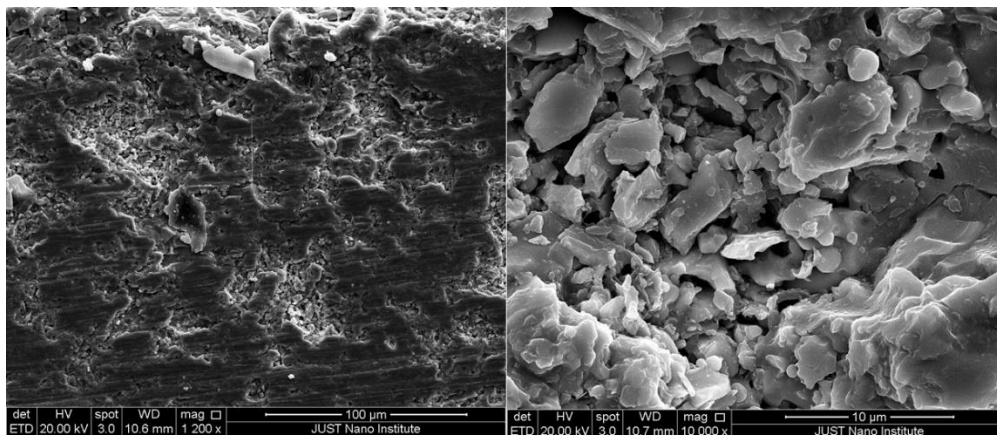


Figure 3. (a) SEM image of the porosities at the YAG topcoat in the as-sprayed condition.
(b) Unmelted particles and granules inside the pores of the as-sprayed YAG top coat.

The porous structure of the coating relieved the tensile stresses that are generated during splat solidification which prevents the propagation of the cracks generated through consecutive splat layers and as a result no vertical cracks were detected in the coating. The granular form of the voids can be explained by the partial melting of large agglomerated particle clusters in the plasma jet during the APS process. The pores and their granular structure serve to reduce the thermal conductivity of the coating due to the strong phonon scattering from the air entrapped in the pores and/or boundaries of unmelted particles [36, 41-44]. Figure 4 shows the EDX spectrum for particles and granules that described above with peaks for the YAG top coat constituent elements Y, Al and O.

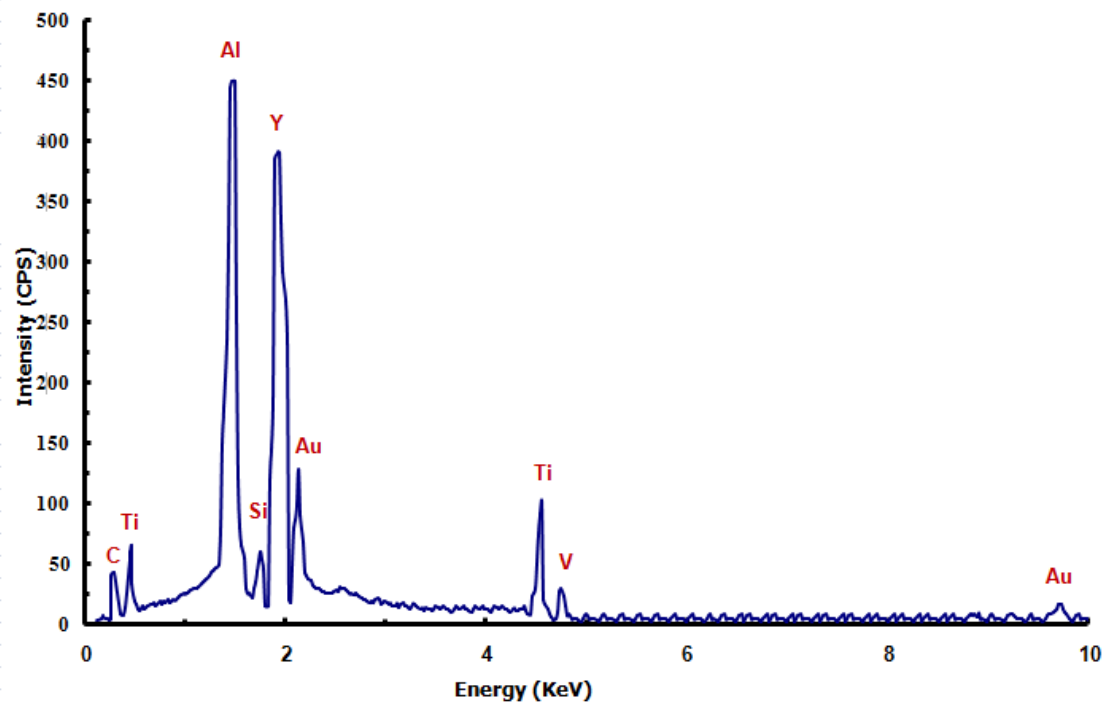


Figure 4. EDX spectrum of pores inside the YAG top coat.

Morphology of the Topcoat's Surface

SEM images of the top coat (YAG) surface show that the surface is rough and filled with cracks, pores and splats that formed during the APS process. The developed splats have different shapes, including disk-shaped splats as those enclosed in the circles and fragmented splats as those enclosed in rectangles in Figure 5. The shape of the as sprayed splats depends on the nature of heat transfer between the solidifying splats and the underlying surface; intermediate cooling causes the splats to have disk shapes while slow cooling results in fragmented splats [45]. The cracks observed can be caused by the relaxation of the cooling stresses generated during splat solidification [23] and/or the shrinkage of the coating's structure accompanies the crystallization of YAG [31]. The elemental analysis of the top coat is shown in Figure 5 and it has the peaks of Y, Al and O.

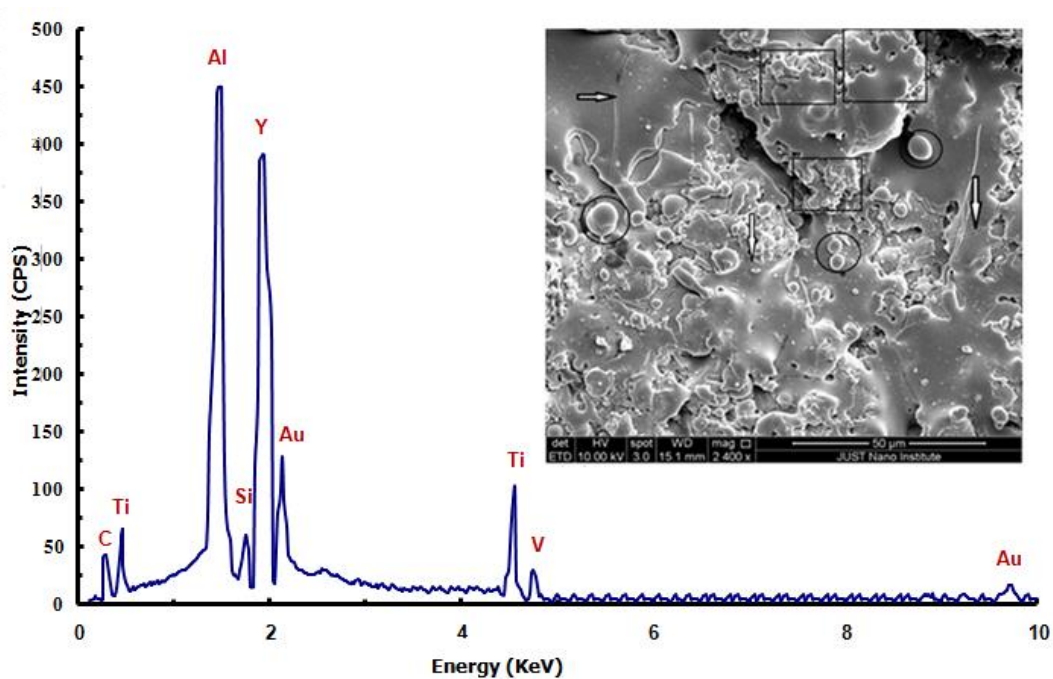


Figure 5. SEM image of splats and EDX spectrum of the as-sprayed YAG topcoat surface.

The shape of the as sprayed splats depends on the nature of heat transfer between the solidifying splats and the underlying surface; intermediate cooling causes the splats to have disk shapes while slow cooling results in fragmented splats [45]. The cracks observed can be caused by the relaxation of the cooling stresses generated during splat solidification [23] and/or the shrinkage of the coating's structure accompanies the crystallization of YAG [31]. The elemental analysis of the top coat is shown in Figure 5 and it has the peaks of Y, Al and O.

Thermal Shock Resistance

The surface of the coating after the thermal shock shows that the coating experienced no spallation at the center and the delamination took place at the edges of the coating as shown in Figure 6, with a spallation area of less than 5% of the coating, delamination at the edges of the coating can be caused by the large stresses due to edge effect and discontinuous coating thickness [29]. Also, cracks and pores can be observed in Figure 6.

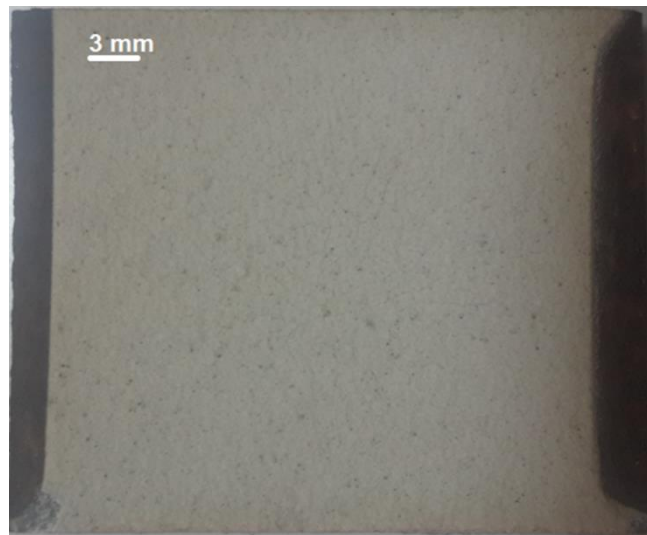


Figure 6. Macro-image of Ti-6Al-4V substrate coated with YAG after thermal shock test for 150 cycles.

The microstructure of the cross-section of the coated samples after 150 cycles of thermal shock test reveals the changes in the microstructure that took place as a result of the test compared to the as sprayed microstructure see Figure 7. The voids and pores in the top coat shown in the as sprayed conditions almost disappeared due to sintering effect because of thermal exposure which increase the thermal conductivity of the coating [46, 47]. Figure 7 also shows interfacial voids between the top and bond coats. The emergence of voids at the bond coat-substrate interface can be seen as well as the cracking at several locations in the bond coat.

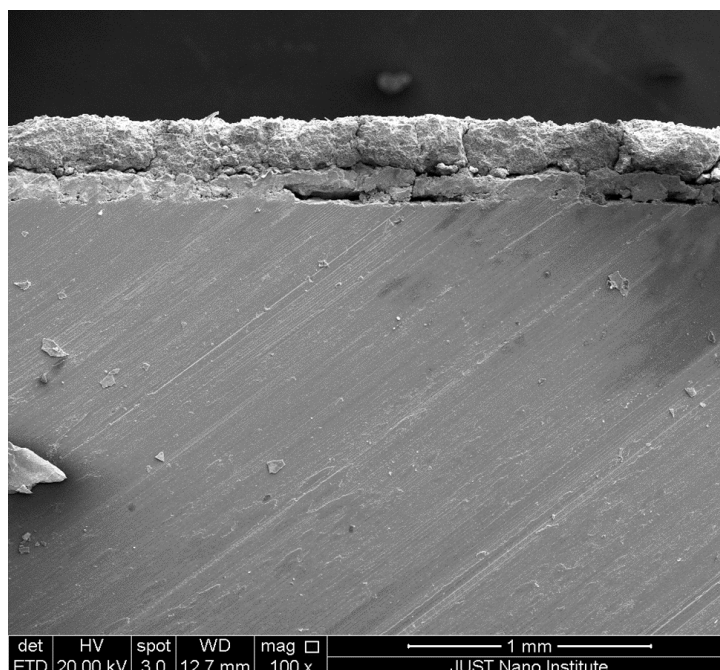


Figure 7. SEM image of the cross-section of the coated Ti-6Al-4V with YAG after 150 cycles.

The coating has both vertical cracks through the total thickness of the top coat (see the rectangles in Figure 8 and the horizontal arrow in Figure 9) and transverse cracks (see the vertical arrow in Figure 9).

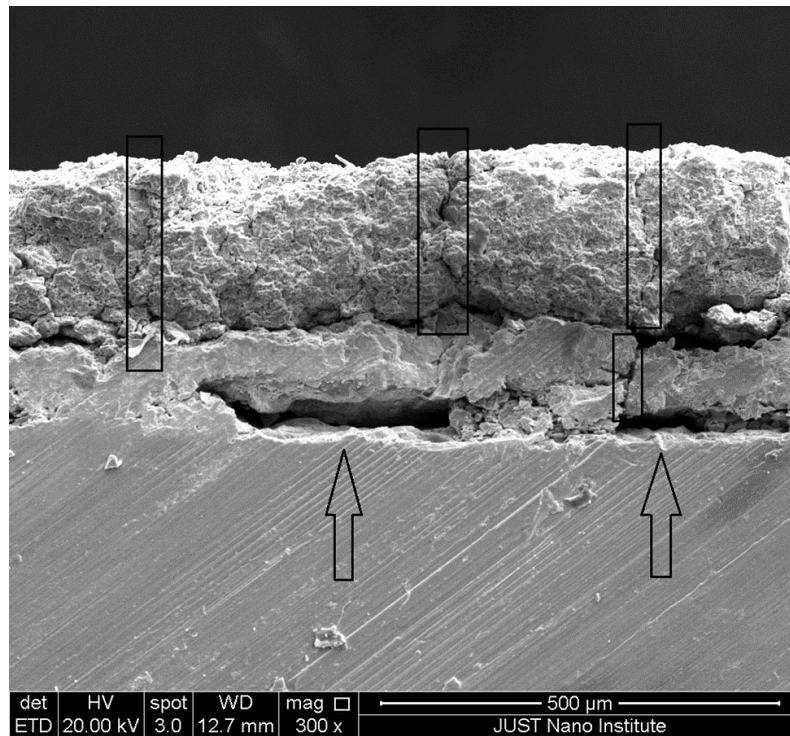


Figure 8. SEM cross-sectional image showing vertical cracks in the coating after thermal shocks.

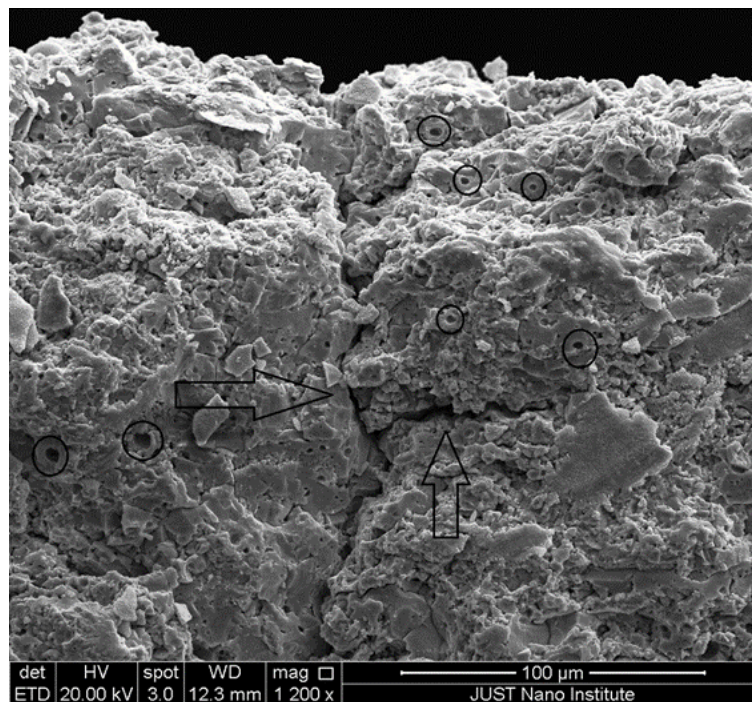


Figure 9. The sintering of the top coat after thermal shocking.

The vertical cracks formation can be explained the propagation of quenching-induced micro-cracks through splat layers induced by thermal stresses that was helped by sintering and the densification of the coating. The transverse cracks are also propagated by induced thermal stresses and negatively affect the coating's thermal shock resistance leading to spallation. Spallation and cracks are caused by thermal stresses generated due to mismatch of thermal expansion coefficient between the substrate and the coating layers. Sample buckling generated compressive stresses which

contributed to spallation and voids generated especially between the substrate and the bond coat (see the arrows in Figure 8).

The effects of sintering are seen in Figures 9 and 10; Figure 9 shows that porosity was largely reduced but small voids can be seen (enclosed in the circles) indicating incomplete sintering of the top coat and Figure 10 shows the reduction of the thickness of the coating due to densification.

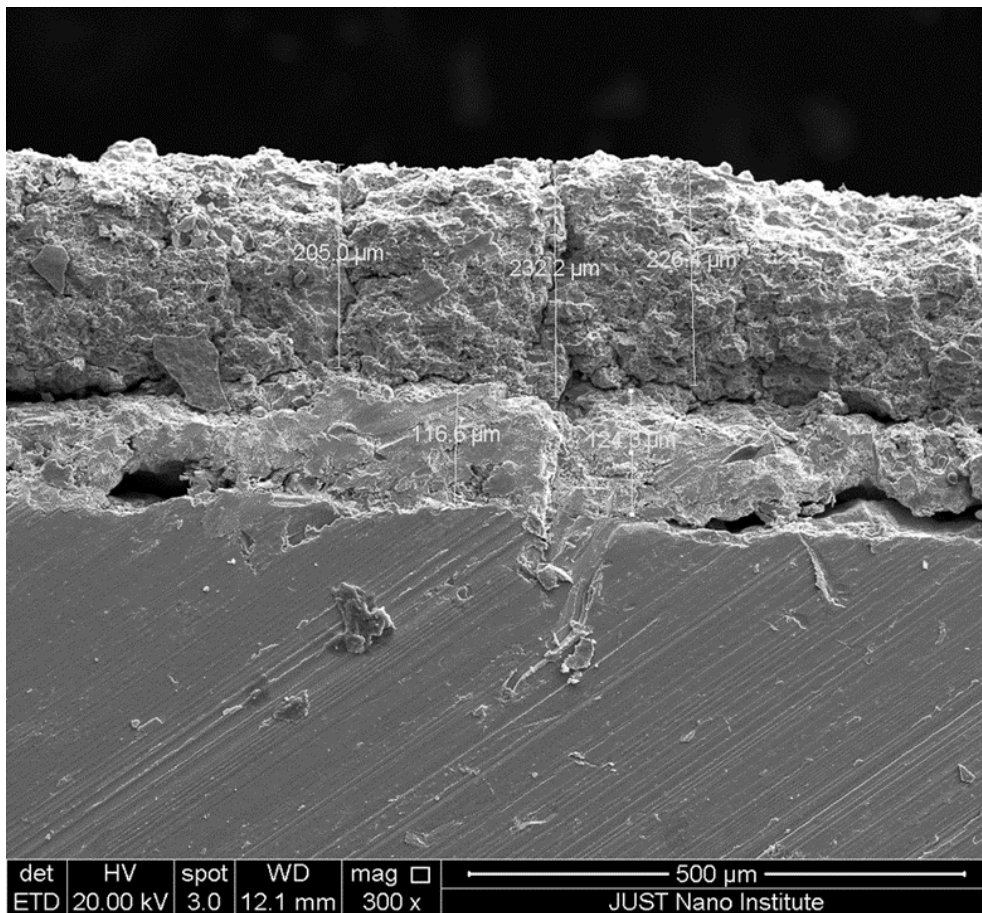


Figure 10. SEM image of the cross-section of the YAG showing thicknesses of the coating after thermal shock cycles.

The morphology of the YAG topcoat surface after thermal shocks is similar to that of the as-sprayed coating. The comparison between the surface of the top coat before and after thermal shocks revealed that the cracks are wide after thermal shocks, where narrower cracks exist at the as-sprayed condition as can be seen in Figure 11; this widening can be attributed to the thermal stresses generated by the sudden temperature changes during the test.

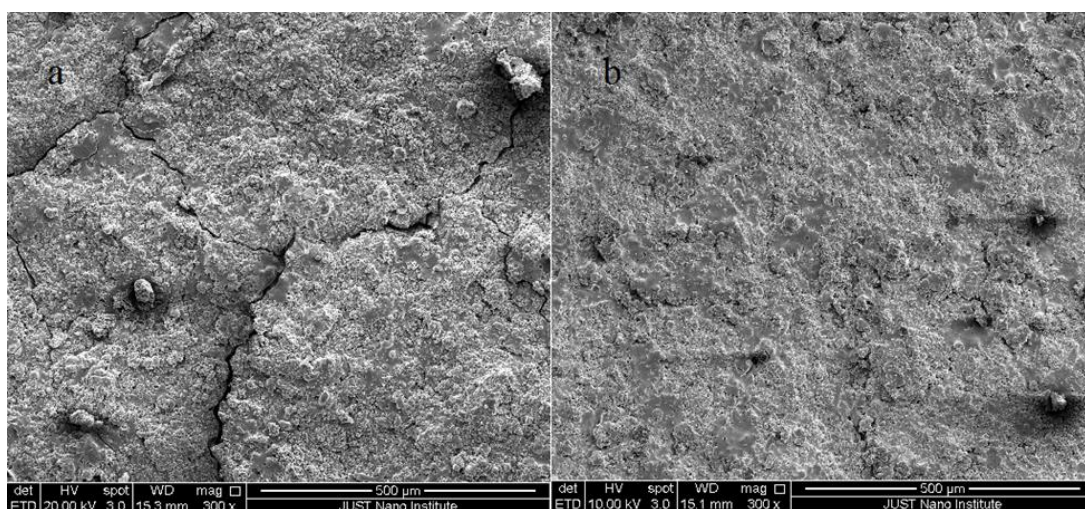


Figure 10. SEM image of the surface of the YAG topcoat at 300X: a) After 150 thermal shock cycles and b) As-sprayed coating.

Crack measurement was conducted for YAG topcoat after the thermal shock test at 5,000 X and 80,000 X showing micro- and nano-sized cracks are shown in Figure 12.

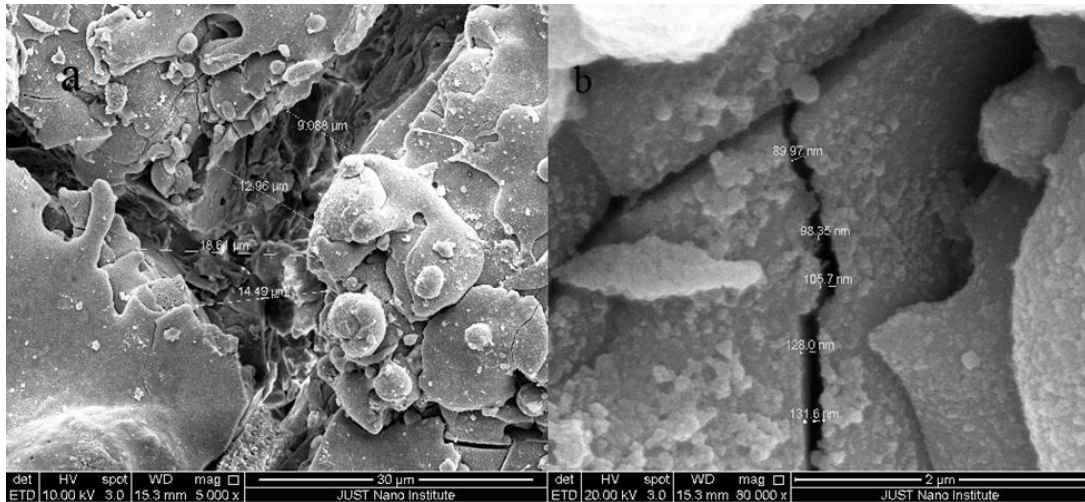


Figure 11. SEM images of the YAG topcoat's surface after the thermal shock test (a) micro-cracks and (b) nano-cracks.

The elemental analysis of the YAG topcoat after the thermal shock indicated the same elements as the as sprayed coating as shown in Figure 13.

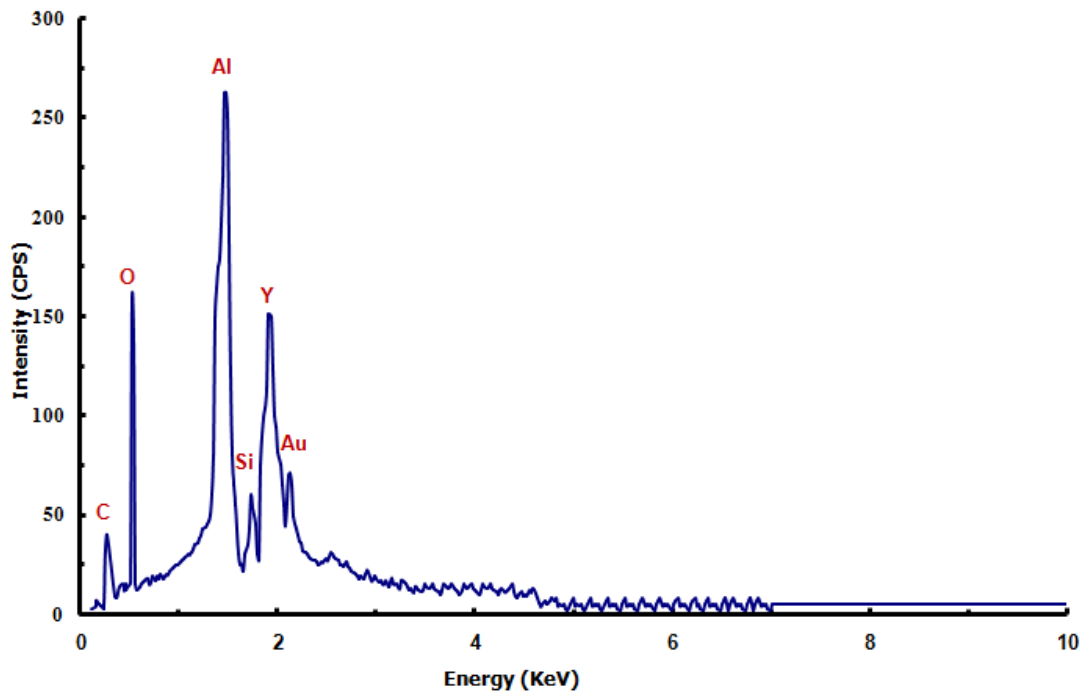


Figure 12. EDX spectrum of the surface of the YAG topcoat after the thermal shock test.

Vickers Hardness Test Results

The average value of the Vickers hardness readings for nine measurements (listed in Table 4) was 331.35 H.V. with standard deviation of 15.06. In this test, 1.0 kg load was used because of the high pores content that were observed in the top coat, as these local variations of the microstructure affect the lower loads [48]. This porous microstructure resulted in the reduction of the hardness as compared with the hardness of the dense bulk YAG which is 1700 HV because it reduces the effective cross sectional of the material and its load bearing capacity[33, 49]. The hardness of the coating plays an important role in its erosion resistance [33, 50].

Table 4. Values of the Vickers hardness test.

Indentation number	Vickers hardness test
1	352.0
2	327.2
3	316.8
4	329.6
5	352.7
6	308.0
7	322.9
8	332.6
9	340.4

Adhesion Strength Test

The results of the coating adhesion strength showed that failure of the coating occurred at the bond coat-substrate interface, as depicted in Figure 2 because of their weak mechanical bonding in comparison with the strong mechanical bonding of the top coat-bond coat attained from high roughness of the bond coat. The tensile stress of the coating was 17.6 MPa. The value was not far from the corresponding reported value for Metco 450 NS of 20.7 MPa in its data sheet on a low carbon steel substrate. This discrepancy may be explained by insufficient surface roughness (see Figure 2) created by sand blasting which can reduce the mechanical bonding between the bond coat and the substrate. In addition to the different chemical composition of the substrates which affect the bonding. However, the surface roughness has more pronounce effect than the chemical composition on the adhesion strength.

CONCLUSIONS

Based on the findings of this work, the following conclusions can be drawn: The operating temperature of titanium alloy Ti-6Al-4V can be increased by applying yttrium aluminum oxide thermal barrier coating using atmospheric plasma spray from 350 °C to 800 °C. The as-sprayed coating has a porous and partially amorphous structure. This structure acts to increase phonon scattering, which reduce thermal conductivity of the TBC. The coating has an excellent thermal shock resistance; as no tangible spallation observed after 150 cycles. Thermal shock of the coating resulted in widened surface cracking, the formation of vertical cross-sectional cracks and the sintering of the coating. The high porosity of the topcoat improves its thermal shock performance, delays its complete sintering and reduces its hardness compared to the dense YAG material.

ACKNOWLEDGEMENTS

Authors express their gratitude to the Deanship of Scientific Research at Jordan University of Science and Technology (J.U.S.T.) for funding this work via the grant no. 390/2016. Thanks are also extended to Jordan Airmotive Company for the valuable technical assistance they provided.

REFERENCES

- [1] Kitashima T, Suresh KS, Yamabe-Mitarai Y. Present stage and future prospects of development of compressor material. *Crystal Research and Technology*. 2015;50(1):28-37.
- [2] Lu M, McCormick P, Zhao Y, Fan Z, Huang H. Laser deposition of compositionally graded titanium oxide on Ti6Al4V alloy. *Ceramics International*. 2018;44(17):20851-20861.
- [3] He B, Li F, Zhou H, Dai Y, Sun B. Microstructure and thermal cycling behavior of thermal barrier coating on near- α titanium alloy. *Journal of Coatings Technology and Research*. 2007;4(3):335-340.
- [4] Khan MAR, Rahman MM, Kadirgama K, Noor MM. Prediction of surface roughness of Ti-6Al-4V in electrical discharge machining: A regression model. *Journal of Mechanical Engineering and Sciences*. 2011;1:16-24.
- [5] Hamdan SH, Said AYM, Biki JR. Surface finish when threading titanium-based alloy under dry machining. *Journal of Mechanical Engineering and Sciences*. 2014;7:1062-69.
- [6] Alfirano A, Friandani SS, Sutowo C. Effect of solution treatment on the microstructure and mechanical properties of Ti-6Al-6Mo hot-rolled alloy. *Journal of Mechanical Engineering and Sciences*. 2019;13(2):4857-4868.
- [7] Xiao Z, Tan F, Wang W, Sun F, Lu H, Qiu X, Chen J, Qiao X. Oxidation protection of Ti-6Al-4V alloy using a novel glass-amorphous silica composite coating. *Ceramics International*. 2014;40(2):3503-3509.
- [8] Dai J, Zhu J, Chen C, Weng F. High temperature oxidation behavior and research status of modifications on improving high temperature oxidation resistance of titanium alloys and titanium aluminides: A review. *Journal of Alloys and Compounds*. 2016;685:784-798.

- [9] He B, Li F, Zhou H, Dai Y, Sun B. Thermal failure of thermal barrier coating with thermal sprayed bond coating on titanium alloy. *Journal of Coatings Technology and Research*. 2008;5(1):99-106.
- [10] Li GR, Xie H, Yang GJ. Scale-progressive healing mechanism dominating the ultrafast initial sintering kinetics of plasma-sprayed thermal barrier coatings. *Ceramics International*. 2018;44 (14) 16732-16738.
- [11] Injeti G. Identification of a smart bond coating for gas turbine engine applications. *Journal of Coatings Technology and Research*. 2008;5(3):385-391.
- [12] Zeng J, Sun J, Zhang H, Yang X, Qiu F, Zhou P, Niu W, Dong S, Zhou X, Cao X. Lanthanum magnesium hexaluminate thermal barrier coatings with pre-implanted vertical microcracks: Thermal cycling lifetime and CMAS corrosion behaviour. *Ceramics International*. 2018;44(10):11472-11485.
- [13] Tailor S, Upadhyaya R, Manjunath SY, Dub AV, Modi A, Modi SC. Atmospheric plasma sprayed 7%-YSZ thick thermal barrier coatings with controlled segmentation crack densities and its thermal cycling behavior. *Ceramics International*. 2018;44(3):2691-2699.
- [14] Chen Z, Huang H, Zhao K, Jia W, Fang L. Influence of inhomogeneous thermally grown oxide thickness on residual stress distribution in thermal barrier coating system. *Ceramics International*. 2018 ;44(14):16937-16946.
- [15] Khan M, Hu N, Zhenhua L, Wang Y, Yi Z. Influence of solution-precursor plasma spray (SPPS) processing parameters on the mechanical and thermodynamic properties of 8 YSZ. *Ceramics International*. 2018;44(7):7794-7798.
- [16] Klement U, Ekberg J, Creci S, Kelly ST. Porosity measurements in suspension plasma sprayed YSZ coatings using NMR cryoporometry and X-ray microscopy. *Journal of Coatings Technology and Research*. 2018;15(4):753-757.
- [17] Lv B, Mücke R, Fan X, Wang TJ, Guillon O, Vaßen R. Sintering resistance of advanced plasma-sprayed thermal barrier coatings with strain-tolerant microstructures. *Journal of the European Ceramic Society*. 2018;38(15):5092-5100.
- [18] Zhang XF, Zhou KS, Liu M, Deng CM, Deng CG, Mao J, Deng ZQ. Mechanisms governing the thermal shock and tensile fracture of PS-PVD 7YSZ TBC. *Ceramics International*. 2018;44(4):3973-3980.
- [19] Hashaikeh R, Szpunar JA. Electrophoretic fabrication of thermal barrier coatings. *Journal of Coatings Technology and Research*. 2011;8(2):161-169.
- [20] Zhou H, Li F, Wang J. Microstructure analyses and thermophysical properties of nanostructured thermal barrier coatings. *Journal of Coatings Technology and Research*. 2009;6(3):383-390.
- [21] Carpio P, Salvador MD, Borrell A, Sánchez E. Thermal behaviour of multilayer and functionally-graded YSZ/Gd₂Zr₂O₇ coatings. *Ceramics International*. 2017;43(5):4048-4054.
- [22] Dhineshkumar SR, Duraiselvam M, Natarajan S, Panwar SS, Jana T, Khan MA. Enhanced ablation resistance through laser glazing of plasma sprayed LaTi₂Al₉O₁₉-based functionally graded thermal barrier coating. *Ceramics International*. 2016;42(8):10184-10190.
- [23] Sun J, Wang J, Zhou X, Dong S, Deng L, Jiang J, Cao X. Microstructure and thermal cycling behavior of plasma-sprayed LaMgAl₁₁O₁₉ coatings. *Ceramics International*. 2018;44(5):5572-5580.
- [24] Padture NP, Klemens PG. Low thermal conductivity in garnets. *Journal of the American Ceramic Society*. 1997;80(4):1018-1020.
- [25] Kim HJ, Fair GE, Hart AM, Potticary SA, Usechak NG, Corns RG, Hay RS. Development of polycrystalline yttrium aluminum garnet (YAG) fibers. *Journal of the European Ceramic Society*. 2015;35(15):4251-4258.
- [26] Pfeifer S, Bischoff M, Niewa R, Clauß B, Buchmeiser MR. Structure formation in yttrium aluminum garnet (YAG) fibers. *Journal of the European Ceramic Society*. 2014;34(5):1321-1328.
- [27] Wang J, Xu F, Wheatley RJ, Neate N, Hou X. Yb³⁺ doping effects on thermal conductivity and thermal expansion of yttrium aluminium garnet. *Ceramics International*. 2016;42(12):14228-14235.
- [28] Xue Z, Ma Y, Gong S, Guo H. Influence of Yb³⁺ doping on phase stability and thermophysical properties of (Y_{1-x}Yb_x)₃Al₅O₁₂ under high temperature. *Ceramics International*. 2017;43(9):7153-7158.
- [29] Saravanan S, Srinivas GH, Jayaram V, Paulraj M, Asokan S. Synthesis and characterization of Y₃Al₅O₁₂ and ZrO₂-Y₂O₃ thermal barrier coatings by combustion spray pyrolysis. *Surface and Coatings Technology*. 2008;202(19):4653-4659.
- [30] Wu Y, Du J, Choy KL. Novel Deposition of Columnar Y₃Al₅O₁₂ Coatings by Electrostatic Spray-Assisted Vapor Deposition. *Journal of the American Ceramic Society*. 2006;89(1):385-387.
- [31] Weyant CM, Faber KT. Processing-microstructure relationships for plasma-sprayed yttrium aluminum garnet. *Surface and Coatings Technology*. 2008;202(24):6081-6089.
- [32] Su YJ, Trice RW, Faber KT, Wang H, Porter WD. Thermal Conductivity, Phase Stability, and Oxidation Resistance of Y₃Al₅O₁₂ (YAG)/Y₂O₃-ZrO₂ (YSZ) Thermal-Barrier Coatings. *Oxidation of metals*. 2004;61(3-4):253-271.
- [33] Gell M, Wang J, Kumar R, Roth J, Jiang C, Jordan EH. Higher Temperature Thermal Barrier Coatings with the Combined Use of Yttrium Aluminum Garnet and the Solution Precursor Plasma Spray Process. *Journal of Thermal Spray Technology*. 2018;27(4):543-555.
- [34] Yang K, Rong J, Feng J, Zhuang Y, Tao S, Ding C. In-situ fabrication of amorphous/eutectic Al₂O₃-YAG ceramic composite coating via atmospheric plasma spraying. *Journal of the European Ceramic Society*. 2016;36(16):4261-4267.
- [35] The International Center for Diffraction Data. ICDD data base. Available at: [http:// www.icdd.com](http://www.icdd.com). Accessed through Rigaku PDXL software.

- [36] Cho J, Park J, An J. Low thermal conductivity of atomic layer deposition yttria-stabilized zirconia (YSZ) thin films for thermal insulation applications. *Journal of the European Ceramic Society*. 2017;37(9):3131-3136.
- [37] Zhan X, Li Z, Liu B, Wang J, Zhou Y, Hu Z. Theoretical prediction of elastic stiffness and minimum lattice thermal conductivity of $Y_3Al_5O_{12}$, $YAlO_3$ and $Y_4Al_2O_9$. *Journal of the American Ceramic Society*. 2012;95(4):1429-1434.
- [38] Thakare JG, Mulik RS, Mahapatra MM. Effect of carbon nanotubes and aluminum oxide on the properties of a plasma sprayed thermal barrier coating. *Ceramics International*. 2018;44(1):438-451.
- [39] Li GR, Cheng B, Yang GJ, Li CX. Strain-induced stiffness-dependent structural changes and the associated failure mechanism in TBCs. *Journal of the European Ceramic Society*. 2017;37(11):3609-3621.
- [40] Di Girolamo G, Marra F, Blasi C, Serra E, Valente T. Microstructure, mechanical properties and thermal shock resistance of plasma sprayed nanostructured zirconia coatings. *Ceramics International*. 2011;37(7):2711-2717.
- [41] Ghai R, Chen K, Baddour N. 2019. Modelling thermal conductivity of porous thermal barrier coatings. *Coatings*. 2019; 9(2): 101-129.
- [42] Hu N, Khan M, Wang Y, Song X, Lin C, Chang C, Zeng Y. Effect of microstructure on the thermal conductivity of plasma sprayed Y_2O_3 stabilized zirconia (8% YSZ). *Coatings*. 2017;7:198- 207.
- [43] Kai W, Hui P, Hongbo G, Shengkai G. Effect of sintering on thermal conductivity and thermal barrier coatings. *Chinese Journal of Aeronautics*. 2012;25: 811-816.
- [44] Rätzer-Scheibe H J, Schulz U. The effects of heat treatment and gas atmosphere on the thermal conductivity of APS and EB-PVD PYSZ thermal barrier coatings. *Surface and Coatings Technology*. 2007;201(18):7880-7888.
- [45] Chandra S, Fauchais P. Formation of solid splats during thermal spray deposition. *Journal of Thermal Spray Technology*. 2009;18(2):148-180.
- [46] Jiang K, Liu S, Wang X. Low-thermal-conductivity and high-toughness CeO_2 - Gd_2O_3 co-stabilized zirconia ceramic for potential thermal barrier coating applications. *Journal of the European Ceramic Society*. 2018;38(11):3986-3993.
- [47] Zambrano DF, Barrios A, Tobón LE, Serna C, Gómez P, Osorio JD, Toro A. Thermal properties and phase stability of Yttria-Stabilized Zirconia (YSZ) coating deposited by Air Plasma Spray onto a Ni-base superalloy. *Ceramics International*. 2018;44(4):3625-3635.
- [48] Davis JR, editor. *Handbook of thermal spray technology*. ASM international (2004).
- [49] Sinha A, Farhat Z. Effect of surface porosity on tribological properties of sintered pure Al and Al 6061. *Materials Science and Applications*. 2016;6(6): 549-566.
- [50] Steinberg L, Naraparaju R, Heckert M, Mikulla C, Schulz U, Leyens C. Erosion behavior of EB-PVD 7YSZ coatings under corrosion/erosion regime: Effect of TBC microstructure and the CMAS chemistry. *Journal of the European Ceramic Society*. 2018;38(15):5101-5112.